Convergent evolution of p38/MAPK activation in hormone resistant prostate cancer mediates pro-survival, immune evasive, and metastatic phenotypes

Kathryn E. Ware[1,2], Santosh Gupta[1,2], Jared Eng[1,2], Gabor Kemeny[1], Bhairavy J. Puviindran[1], Wen-Chi Foo[3], Lorin A. Crawford[4], R. Garland Almquist[1], Daniella Runyambo[1], Beatrice C. Thomas[1], Maya U. Sheth[1], Anika Agarwal[1], Mariaelena Pierobon[5], Emanuel F. Petricoin[5], David L. Corcoran[1], Jennifer Freedman[1,2], Steven R. Patierno[1,2], Tian Zhang[1,2], Simon Gregory[1], Zoi Sychev[6], Justin M. Drake[6,7,8], Andrew J. Armstrong[1,2,9]*, and Jason A. Somarelli[1,2]*, *=co-corresponding authors

Affiliations: [1]Department of Medicine, Division of Medical Oncology, Duke University Medical Center, Durham, NC; [2]Duke Cancer Institute Center for Prostate and Urologic Cancers, Duke University Medical Center, Durham, NC; [3]Department of Pathology, Duke University Medical Center, Durham, NC; [4]Department of Biostatistics, Brown University, Providence, Rhode Island; [5]Center for Applied Proteomics and Molecular Medicine, George Mason University, Fairfax, Virginia; [6]Department of Pharmacology and [7]Urology, University of Minnesota, Minneapolis, MN. [8]Masonic Cancer Center, University of Minnesota, Minneapolis, MN; [9]Department of Pharmacology and Cancer Biology, Duke University, Durham NC

Correspondence: jason.somarelli@duke.edu; andrew.armstrong@duke.edu

Summary (120 words)

Adaptation of cancer cells to targeted therapy follows ecological paradigms observed in natural populations that encounter resource depletion and changing environments, including activation of pro-survival mechanisms, migration to new locations, and escape of predation. We identified the p38 MAPK pathway as a common molecular driver of these three responses during the adaptation to hormone therapy resistance in prostate cancer. The p38 pathway is activated in therapy-resistant cells and mechanistically drives these three convergent responses through sustained AR activity, enhanced invasion and metastasis, and immune evasion. Targeting p38 signaling may represent a new therapeutic strategy to treat men with metastatic, hormone therapy-resistant prostate cancer.

Keywords

drug resistance; androgen receptor; enzalutamide; prostate cancer; phenotypic convergence; convergent evolution; Snail; castration resistance; PD-L1

Introduction

Populations of individuals within an ecological niche must acquire the necessary resources to survive and propagate their genetic material to the next generation. Individuals have adapted a wide range of strategies to ensure resource acquisition in an ever-changing environment. Some of these strategies include dormancy (Varpe, 2017), hibernation (KIlduff, 2004), migration, and avoidance of predation (Skov et al., 2010).

Cancer cells adapt similar strategies within the context of the ecological niche of the body to cope with variations in resource availability that promotes their survival. A major resource for cancer cells is the oncogene signaling pathway to which they are addicted. For prostate cancer cells, this critical lineage oncogene is most often the androgen receptor (AR) (Mills, 2014). AR activity is pharmacologically targeted through blocking the ligand binding domain or inhibition of androgenic ligand biosynthesis. Enzalutamide, a 2nd generation inhibitor of the androgen receptor, and abiraterone acetate, an androgen synthesis inhibitor, each delay progression and improve the survival of men with both early and late castration-resistant prostate cancer (Beer et al., 2014; de Bono et al., 2011; Penson et al., 2016; Ryan et al., 2013; Scher et al., 2012). These potent hormonal therapies significantly prolong the overall survival of men with metastatic, castration-resistant prostate cancer; however, acquired resistance to these drugs over a median of one to two years is inevitable.

Upon disease progression with enzalutamide or abiraterone treatment, most tumors remain AR dependent and have a rise in serum levels of prostate-specific antigen (PSA) (Bluemn et al., 2017; Bryce et al., 2017). Multiple mechanisms of AR signal restoration have been identified that directly impact the AR gene, including AR amplification, AR mutations, genomic structural rearrangements (Li et al., 2011b; Li et al., 2012; Liu et al., 2013; Ware et al., 2014), and alternative splicing events (Liu et al., 2014). Additionally, alternative mechanisms can promote the AR transcriptome or promote AR activity through substitute methods of AR activation (Arora et al., 2013; Ware et al., 2014) to generate a pro-survival response (Chen et al., 2004; Viswanathan et al., 2018).

In addition to AR activation, complementary pro-survival responses focus on metabolic plasticity, such as dormancy and hibernation. Cancer cells adapt their energetic needs to accompany survival and fitness in hostile environments (Lehuede et al., 2016), and disseminated tumor cells can be found in many prostate cancer patients prior to any clinical symptoms (Ruppender et al., 2013; van der Toom et al., 2016). Furthermore, organisms and cancer cells alike must avoid predation to ensure their survival in any environment. Prostate cancer cells avoid the predation of the immune system in a number of ways, including 1) secretion of immunosuppressive molecules, such as TGF-β (Yang et al., 2010; Yoshimura and Muto, 2011) and soluble WNT ligands (Robinson et al., 2015), and 2) expression of cell surface or cellular immune checkpoint molecules (Antonarakis et al., 2020; Gao et al., 2017; Graff et al., 2016). For example, TGF-β has been identified as a potent immunosuppressive ligand, which can be regulated through Snail to mediate downregulation of HLA-I and promote immune escape (Chen et al., 2015). Similarly, the immunosuppressive ligand PD-L1 is upregulated in response to enzalutamide-resistant progression, both in tumor cells and in circulating immune subsets (Bishop et al., 2015; Graff et al., 2016). Additionally, we have shown that PD-L1 expression is more prevalent on circulating tumor cells from metastatic prostate cancer patients who are progressing on abiraterone acetate or enzalutamide treatment (Zhang et al., 2018).

In the present study we sought to understand the adaptations to hormone therapy resistance in prostate cancer. Using an integrated genomics approach we observed that enzalutamide-induced AR signaling blockade induces convergent phenotypic evolution on three ecological responses: 1) altered resource acquisition to promote cellular

persistence and survival through oncogene re-activation, 2) upregulation of migratory/invasive factors, and 3) avoidance of predation by immune evasion and immune suppression (**Fig. 1**). All three of these phenotypes converge across different model systems on the p38/MAPK stress response pathway, which is highly activated in human prostate cancer metastases and can be therapeutically leveraged to simultaneously target and limit these pro-survival responses to overcome enzalutamide resistant growth and survival.

Results

Enzalutamide resistant cells exhibit diverse genomic adaptations

Enzalutamide is a potent inhibitor of AR activity (Tran et al., 2009) that initially induces a response in most men with metastatic castration resistant prostate cancer; however, progression on enzalutamide typically develops within 1-2 years (Beer et al., 2014). A deeper understanding of the mechanisms underlying the evolution of enzalutamide resistance is needed to target these resistance mechanisms. To identify common molecular mechanisms of enzalutamide resistance we developed a panel of four enzalutamide-resistant (enzaR) cell lines, LNCaP-enzaR, CS2-enzaR, LN95-enzaR, and MDA-PCa-2b-enzaR, by chronic, long-term exposure to increasing doses of enzalutamide. For LNCaP and MDA-PCa-2b cells, the cells were initially exposed to 1 μM enzalutamide and allowed to grow to confluence. The dose of enzalutamide was doubled at each subsequent passage until cells were capable of sustained growth in the presence of 50 μM enzalutamide (**Fig. 2A**), which is above the concentration observed in men with metastatic, castration resistant prostate cancer (Scher et al., 2010). In parallel

with development of these enzalutamide-resistant models, we also created enzalutamide-resistant populations of LNCaP sublines, CS2 and LN95. Both CS2 and LN95 (Hu et al., 2012) cells were first adapted to androgen deprivation therapy (ADT) by passaging in media supplemented with an increasing ratio of androgen-depleted media. Following evolution of ADT resistance, cells were then adapted to enzalutamide with increasing doses as described above (**Fig. 2A**). All enzaR cell lines are characterized by a significant increase in cell growth and a decrease in apoptosis in response to enzalutamide treatment (**Fig. 2B**).

Analysis of these enzaR cells revealed several clinically-relevant genotypes and phenotypes. All cell lines had persistent AR expression (**Fig. 2C-D**) and did not have notable morphologic changes or consistent neuroendocrine differentiation (**Supplementary Fig. S1A)**. The enzalutamide-resistant LNCaP model acquires the F876L mutation in AR that converts enzalutamide into a partial agonist (Balbas et al., 2013; Korpal et al., 2013) (**Supplemental Fig. S2)**, but lack additional novel AR mutations. The enzaR LNCaP and CS2 cells express full-length AR, but do not produce the AR splice variant, AR-V7, which is a known enzalutamide-resistance driver (Antonarakis et al., 2014) (**Fig. 2C-E**). On the other hand, enza-R LN95 cells upregulate both full length AR and AR-V7 (**Fig. 2C-E**). Enza-R CS2 cells display upregulation of the glucocorticoid receptor mRNA and genomic loss of *RB1* and *BRCA2*, which are known drivers of resistant and aggressive prostate cancer (Arora et al., 2013; Chakraborty et al., 2019). None of these lines have upregulation of biomarkers of neuroendocrine lineage plasticity as measured by co-*RB1* and *TP53* genomic loss or transcriptional upregulation of *SOX2*, and none of these lines expresses markers of neuroendocrine

lineage plasticity (Mu et al., 2017) at the mRNA level (**Supplemental Fig. S1B**). We also did not observe changes in the stemness markers *CD133*, *NANOG*, or *OCT4* in the enzaR cell lines (**Fig. 2E, Supplemental Fig. S3**). Thus, this panel of cell lines parallels the heterogeneous spectrum of AR-positive prostate cancer phenotypes most commonly observed in the clinic upon progression on enzalutamide.

To further understand the evolution of enzalutamide resistance in these heterogeneous models of prostate cancer, we analyzed the genome, transcriptome and phospho-proteome of these paired cell lines prior to enzalutamide exposure and following adaptation to enzalutamide resistance. Genetically, the enzaR models were all remarkably unique. While enzaR CS2 and LN95 cells share just one copy number alteration – a gain in chromosome 20p13-p11.1 – this gain is not present in enzaR LNCaP cells (**Supplemental Fig. S4**). Likewise, enzaR models acquired relatively few single nucleotide variants in the exome between paired parental and enzaR cell lines, and of these alterations, none were shared across all enzaR cells (**Supplemental Fig. S5A-B**). Together, these data suggest that the enzaR lines do not harbor shared genetic alterations that contribute to their adaptation to enzalutamide.

Enzalutamide resistance converges on MAPK signaling and stress response pathways

Given the diversity of genetic lesions in the enzaR models, we next sought to determine the molecular drivers underlying the evolution of enzalutamide resistance. Across each parental and resistant model system, we performed whole transcriptome RNA Sequencing to identify consistent changes in RNA expression and pathways

associated with resistance. Similar to our DNA-level analyses, we observed relatively few gene expression changes common to all cell line models (4-5% overlap; **Fig. 3A**). We also performed a reverse phase protein array (RPPA) and evaluated a subset of proteins and phosphoproteins that are implicated in cancer progression (Akbani et al., 2014). The proteomics data revealed phospho-p38, a key signaling node in the cellular stress response, as the top upregulated phospho-protein in all three enzaR cell lines (**Fig. 3C**). Reanalysis of our RNA-Seq data at the pathway level revealed common transcriptional enrichment of MAPK signaling, DNA repair, and several stress-response pathways (**Fig. 3B**). Importantly, we observed the same enrichment of stress-response pathways and MAPK signaling in a fourth enzalutamide-resistant cell line, MDA-PCa-2b (**Fig. 3D, E**). MDA-PCa-2b is an independent androgen responsive and AR positive prostate cancer cell line. These data suggest that AR-positive enzaR cells exhibit unique genetic and transcriptional landscapes at the gene level that converge on p38 signaling and stress response signaling at the pathway level. These pathways are activated as a consequence of adaptation to enzalutamide and not an acute response, as a short-term (5 day) treatment with enzalutamide does not activate this same p38-mediated response pathway (**Supplemental Fig. 6B**). This pathway-level convergence is reminiscent of convergent evolution observed in ecological contexts during resource depletion, including the conserved activation of the p38 MAPK pathway itself (Gatenby et al., 2011; Harrison et al., 2004; Li et al., 2011a).

Considering the convergent evolutionary behavior of the enzaR cells at the gene expression/signaling levels, we next attempted to better understand if these changes also promoted phenotypic convergence during the acquisition of enzalutamide resistance. To

do this, we first explored the phenotypic consequences of p38/MAPK pathway activation. The p38/MAPK pathway is a key regulator of the stress response (Igea and Nebreda, 2015), and a regulator of tumor cell dormancy in many cancer types, including prostate cancer (Decker et al., 2017; Yu-Lee et al., 2018). Consistent with the role of p38 in a dormancy phenotype, enzaR cells exhibited a significant downregulation in the ratios of pERK:p38α, an important indicator of the shift from a proliferative (high ERK) to dormant (high p38α) phenotype (**Supplemental Fig S7A**). Likewise, enzaR cells also upregulated p21, a cyclin dependent kinase inhibitor induced during stress response to regulate cell cycle progression (Sosa et al., 2011) (**Supplemental Fig S7B**). Interestingly, unlike enzalutamide-sensitive cells that induce beta-galactosidase activity, a marker of dormant cells, enzaR cells do not increase beta-galactosidase activity in response to enzalutamide treatment. However, enzaR cells have a higher baseline level of beta-galactosidase activity compared to enzalutamide sensitive cells (**Supplemental Fig S7C**). These data suggest that cells adapt to survival during enzalutamide treatment by regulating cell cycle progression and escaping from treatment induced dormancy programs.

Activation of p38/MAPK is enriched in metastatic disease and drives cell growth in prostate cancer

Our results indicate that enzaR cells converge on p38 activation, which is functionally associated with dormancy and a pro-survival phenotype. Prior work has suggested activation of the p38 pathway in disseminated prostate and breast cancer cells from patients (Chery et al., 2014; Werden et al., 2016). Based on our preclinical data and

these observations, we hypothesized that p38 activation would be associated with aggressive and metastatic disease. To test our hypothesis we compared, by immunohistochemistry, 30 primary tumors and 20 metastatic biopsies from prostate cancer patients (Ware et al., 2016) for phospho-p38 expression. These tumors were all positive for AR expression. Importantly, as compared to localized prostate cancer, metastases show a strong activation of p38 (**Fig. 3F**).

To validate these findings, we performed kinase substrate enrichment analysis (KSEA) on our published phosphoproteomic dataset (Drake et al., 2016) consisting of 16 metastatic prostate cancer patients. KSEA demonstrated significantly enriched hyperphosphorylation of p38 substrates in metastatic castration-resistant prostate cancer (CRPC) tissues compared to localized hormone-naïve prostate cancer tissue (**Fig. 3G, Supplemental Table 1**). Independent data sets analysis shows p38 activation as the central hub of cell signaling convergence in human prostate cancer metastases, particularly during the evolution of metastasis and hormone therapy resistance.

Next, we tested whether inhibition of p38 signaling impacted cell growth in our models of enzalutamide resistance. In all enzaR cell line models, treatment with a small molecule p38 inhibitor (SB203580) led to a significant decrease in cell proliferation over time (**Fig. 4A-C**). These data highlight the p38 signaling pathway as important and activated in enzalutamide resistant prostate cancer.

Activation of p38/MAPK promotes sustained AR signaling in the presence of enzalutamide

Previous studies have shown that enzalutamide induces lineage reprogramming toward an AR null, neuroendocrine-like phenotype (Ku et al., 2017; Mu et al., 2017; Paranjape et al., 2016). However, neither the RNA-Seq nor qRT-PCR analyses revealed consistent changes in neuroendocrine biomarkers across our four paired enzalutamide resistant cell lines (**Supplemental Fig. 4**). On the contrary, all enzaR cell line models maintain AR protein expression (**Fig 2C, D**), indicating that phenotypic shifts to AR-null (Bluemn et al., 2017) or neuroendocrine lineages (Aparicio et al., 2011; Dardenne et al., 2016) have not occurred in our four model systems. Thus, our models may recapitulate the common occurrence of AR positive metastatic castration-resistant prostate cancer post-abiraterone/enzalutamide, observed in the majority (>60-70%) of men with lethal prostate cancer (Bluemn et al., 2017) (**Fig. 2**). Consistent with this, treatment with androgen (R1881) induces AR activity as measured by PSA expression (**Fig. 4D-F**), implying that enzaR cells remain androgen dependent and responsive to AR signaling.

To understand how enzalutamide-induced p38 activation may impact AR activity, we treated control and enzaR cells with the p38 inhibitor, SB203580. Inhibition of p38 led to dramatic down regulation of AR activity in both sensitive and resistant cell lines, which suggests p38 plays a role in promoting AR activity in the setting of CRPC. Additionally, treatment with the p38 inhibitor, SB203580, partially blocked androgen-stimulated *PSA* and *NKX3.1* expression (**Fig. 4D-F, S6A**). Taken together, our data indicates p38 activation promotes convergent AR-dependent enzalutamide resistance, at least in part, by facilitating persistent AR activation.

252 To further validate the importance of p38 signaling in promoting enzalutamide
253 resistant growth we performed population-level p38 knockout or p38 constitutive
254 activation in LNCaP and LN95 cells. CRISPR/Cas9-mediated knockout of p38 delayed
255 outgrowth of enzalutamide-resistant cells (**Fig. 5A, B**) and constitutive activation of p38
256 promoted resistance to enzalutamide treatment (**Fig. 5C, D**). Likewise, treatment with the
257 p38 inhibitor, SB203560, *in vivo* significantly reduced the growth of enzaR xenografts
258 (**Fig. 4G**). Consistent with the decreased tumor growth over time, histology from tumor
259 tissues treated with the p38 inhibitor indicated acute inflammation and necrosis with little
260 viable tumor compared to diluent (control) treated tumors (**Fig 4H**). Together, these data
261 suggest a causal mechanistic relationship between p38 activation and acquired resistance
262 to AR inhibition in prostate cancer that can be overcome by p38 blockade *in vivo* and
263

264 **A p38/MAPK axis induces pro-metastatic and immuno-evasive phenotypes**

265 The observation that p38 activity was increased in metastatic tissues suggested
266 that p38 may facilitate metastatic progression or is upregulated during the metastatic
267 cascade. To better understand the mechanisms by which p38 activity may promote
268 metastasis, we interrogated known drivers of metastatic prostate cancer. One of these
269 drivers of metastasis is Snail, a master regulator of epithelial plasticity that promotes
270 migration and invasion and is strongly expressed in 100% of metastatic prostate cancer
271 biopsies (Ware et al., 2016). We have previously shown that Snail activates AR nuclear
272 localization to drive plasticity, invasion, and enzalutamide resistance (Ware et al., 2016).
273 Snail has also been implicated in epithelial plasticity and loss of AR activity in prostate
274 cancer models of AR therapy resistance as well through direct binding to the AR gene

locus (Miao et al., 2017). We observed Snail upregulation in the p38-activated, enzalutamide-resistant cell lines (**Fig. 6A**) as compared to enzalutamide sensitive models, suggesting that enzalutamide-induced p38 activation induces Snail upregulation. Consistent with Snail upregulation, enzalutamide-resistant cells displayed an increase in repressive phosphorylation at serine 9 on the upstream Snail destabilizing protein and known p38 target, GSK3β (Bikkavilli et al., 2008) (**Supplemental Fig. S8A**). These results provide a mechanistic link connecting p38 activation to increased Snail through suppression of GSK3β activity, which may lead directly to altered AR activity and nuclear localization.

Prior studies have demonstrated an association between enzalutamide resistance and PD-L1 expression on tumor and immune cells, as well as the potential benefits of combined enzalutamide and PD-1 inhibition (Bishop et al., 2015; Graff et al., 2016; Zhang et al., 2018), suggesting a connection between AR inhibition and immune evasion. Interestingly, we also observed a significant positive correlation in gene expression data in prostate cancer tissues from The Cancer Genome Atlas between Snail expression and expression of the immune checkpoint molecule, PD-L1 (**Fig. 6B**). To identify Snail as an effector molecule upstream of PD-L1 expression, we used an inducible system to activate Snail in LN95 prostate cancer cells (Ware et al., 2016). Snail activation led to upregulation of PD-L1 mRNA and protein (**Fig. 6C, D**). We also noted common upregulation of PD-L1 by reverse phase protein array analysis, qPCR, and western blotting in all enzaR models as compared to the parental models (**Fig. 7A-C**).

Given the positive relationship between p38 phosphorylation, PD-L1, and Snail expression in both our models and clinical samples, we next sought to determine the

mechanistic links between p38, Snail, and PD-L1. To do this we assessed the consequence of inhibiting or activating p38 signaling on Snail and PD-L1 expression. Remarkably, p38α knockdown led to downregulation of both Snail and PD-L1 (**Fig. 7D**) and constitutive activation of p38α induced Snail and PD-L1 upregulation (**Fig. 7E**). These experiments suggest that p38 activation can promote a pro-metastatic, immune evasive phenotype by stabilizing Snail expression (Ryu et al., 2019) and leading to downstream PD-L1 upregulation. Together, our data suggest that p38 may provide a common mechanistic explanation for evolutionary convergence of cancer cell survival, metastasis, and immune evasion phenotypes in AR positive metastatic castration-resistant prostate cancer, which could be therapeutically targeted through p38 blockade to treat men with hormone therapy resistant prostate cancer (**Fig. 7F**).

Discussion

Hormone therapy-resistant prostate cancer cells undergo convergent evolution onto a pro-survival, metastatic, immuno-evasive gene regulatory network

Our integrated, multi-omics analysis of the evolution of enzalutamide resistance in prostate cancer revealed consistent activation of the p38/Snail/PD-L1 gene regulatory network in the context of persistent AR expression and activity. Activation of this gene expression pathway was observed in the face of heterogeneous and unique acquired genetic landscapes across the diverse model systems tested. Likewise, our current and previous clinical analyses revealed upregulation of both p38 and Snail in metastases from metastatic castration-resistant prostate patients (Ware et al., 2016), all of which are likely to harbor substantial spatial and temporal genetic heterogeneity. This phenotypic

similarity is reminiscent of convergent evolution in natural systems in which strong selective pressures lead to optimal adaptive phenotypes, such as the independent evolution of flight and the loss of sight in low-light environments across multiple, genetically-distinct taxonomic lineages (Gatenby et al., 2011). These results suggest that, in addition to known genetic drivers of resistance (Azad et al., 2015; Ku et al., 2017; Mazrooei et al., 2019; Mu et al., 2017; Romanel et al., 2015), the evolution of resistance can also be mediated by gene regulatory phenotypes rather than any common genetic driver. This convergent evolution into critical molecular driver pathways may be overlooked through the analysis of DNA or RNA-based sequencing approaches in isolation.

The p38/Snail signaling axis promotes cell-intrinsic enzalutamide resistance and metastasis

Eukaryotic cells have evolved to respond to environmental stressors through a robust and highly-coordinated stress response system (Sun and Zhou, 2018). This system is dynamically regulated through multi-level regulation of gene expression networks, which induce reversible phenotypic changes to enable cellular responses.

In the context of cancer, cells encounter a range of environmental stressors, such as hypoxia, reactive oxygen species, glucose and nutrient deprivation, and mechanical stress (reviewed in (Chen and Xie, 2018). In addition to these microenvironmental factors, cancer therapy dramatically alters the environment and induces a range of cellular responses to enable cell survival in the face of therapy-induced resource depletion. One of these key cellular responses is p38/MAPK pathway activation. The p38 pathway is an

evolutionarily-conserved stress response system (Li et al., 2011a), which is responsible for transducing stress signals, such as DNA damage, reactive oxygen species, cytokines, and changes in osmotic pressure, from the extracellular environment to activate transcriptional response programs (Coulthard et al., 2009). Activation of the p38/MAPK pathway has been implicated in numerous cancers, including metastatic prostate cancer (Drake et al., 2016; Khandrika et al., 2009; Koul et al., 2013). Consistent with its role in mediating cellular stress responses, we found that p38 promotes cell-intrinsic resistance to enzalutamide by promoting reactivation of AR activity. Mechanistically, we observed increased phosphorylation of GSK3β at serine 9 (**Supplemental Fig. 8**), which leads to inactivation of GSK3β activity and induces upregulation of Snail. This model is supported by previous reports, which have demonstrated that p38 inhibits GSK3β through phosphorylation (Thornton et al., 2008), which can lead to Snail stabilization (Zhou et al., 2004). Importantly, we have demonstrated that Snail contributes to enzalutamide resistance via upregulation of AR activity (Ware et al., 2016).

In addition to its functions in enzalutamide resistance, p38 and Snail also drive a pro-metastatic and death-resistant phenotype in prostate cancer. Consistent with this, inhibition of p38 leads to reduced survival, clonogenicity, and invasion in prostate cancer cells (Khandrika et al., 2009). Others have also shown that activation of p38 induces TGF-β-mediated Snail upregulation and invasion (Medici et al., 2011). Similarly, we previously demonstrated that Snail is strongly elevated in metastatic, castration-resistant prostate cancer compared to primary prostate cancer (Ware et al., 2016). We also found that Snail activation leads to enhanced migration and invasion of prostate cancer cells

(Ware et al., 2016). In the current study, we define a mechanistic connection between the p38 pathway and Snail that drives enzalutamide resistance and metastasis.

The p38/Snail axis promotes cell-extrinsic immune evasion

Coupled with their roles in enzalutamide resistance, our data suggest the p38/Snail pathway may also contribute to immune evasion by upregulating the immune checkpoint molecule, PD-L1. In addition, enzalutamide exposure alone leads to upregulation of Snail and PD-L1 (Bishop et al., 2015), and our data demonstrates Snail activation can upregulate PD-L1 expression. Consistent with this, PD-L1 is upregulated on melanoma cells through activation of p38 (Noh et al., 2015), providing further strong support for our hypothesis that the p38/Snail axis drives PD-L1 expression. Similarly, in both chronic viral infections and cancer, p38 activation has been linked to inhibition of Stimulator of IFN genes (STING) expression, enhanced CXCR2-mediated myeloid derived suppressor cell activity, and immune evasion (Chen et al., 2017; Wang et al., 2006; Zhang et al., 2017). Together, these findings suggest that p38 and/or immune checkpoint blockade may be therapeutically efficacious in the post-enzalutamide setting. In support of this notion, Graff et al. observed rapid reductions in prostate specific antigen and radiographic responses in approximately ~20% of men with enzalutamide resistant metastatic castration-resistant prostate treated with a combination of the anti-PD-1 therapy pembrolizumab and enzalutamide (Graff et al., 2016; Graff et al., 2018). Furthermore, PD-L1 can indirectly activate p38 through DNA-PKcs, which promotes chemoresistance (Wu et al., 2018), and therefore suggests a common feed forward loop that may connect PD-L1 expression, DNA repair and pro-metastatic pathways (Goodwin

et al., 2015), and convergent p38 activity. Interestingly, PD-L1 expression in the tumor and tumor microenvironment is also associated with poor outcomes and an aggressive and metastatic phenotype in many cancer subtypes (Kim et al., 2016; Wang et al., 2018).

Beyond enzalutamide resistance

The current work highlights the role of the p38 pathway in promoting enzalutamide resistance in prostate cancer. However, the importance of the p38 pathway as a general stress response to any unfavorable environment may suggest the potential of targeting the p38 pathway in other resource-limiting settings in cancer. Indeed, our clinical data suggest that the p38/Snail pathway is induced during metastasis even prior to androgen deprivation or enzalutamide treatment. Therefore, tumor cells undergoing a stress response independent of enzalutamide or prostate cancer may also rely on p38 activation to persist and survive in ecologically-unfavorable environments, such as the hostile environment of the bloodstream during dissemination, or during treatments that target other oncogenic drivers across different cancer types. For example, p38 activity has been shown in both breast and lung cancer to promote chemotherapy resistance (Flem-Karlsen et al., 2019; Liu et al., 2016; Lu et al., 2018). Activation of p38 has also been linked to DNA repair (Canovas et al., 2018), which is also enriched in our models of enzalutamide resistance (**Fig. 3B**). Therefore, p38 inhibition in combination with chemotherapeutic drugs that induce chromosome instability may have therapeutic potential. These data suggest there may be clinical utility in re-purposing p38 inhibitors for the investigation of reversing treatment resistance in metastatic castration-resistant prostate and other cancers (**Fig. 7F**).

Acknowledgements

Funding: This work was supported by grants NIH F32 CA192630 (K.W. Ware), NIH 1R01CA233585-01 (A.J. Armstrong), NIH P30 CA014236 (M. Kastan), Department of Defense W81XWH-18-1-0189 (J.A. Somarelli), Triangle Center for Evolutionary Medicine (J.A. Somarelli), Astellas Scientific and Medical Affairs (A.J. Armstrong), and the Prostate Cancer Foundation (A.J. Armstrong; J.A. Somarelli). Prostate Cancer Foundation Young Investigator Award (J.M. Drake)

The authors thank Drs. William Eward and Everardo Macias for sharing their IncuCyte systems to monitor cell growth and apoptosis over time as well as the core research facilities involved in this work (Duke Functional Genomics, Duke Biorepository & Precision Pathology, Duke Genomic Analysis and Bioinformatics). We would also like to thank Medivation/Astellas for providing the AR inhibitor, enzalutamide.

Author Contributions

Conceptualization, KEW, JAS, AJA; Methodology, KEW, JAS, AJA, DLC, MP, EFP, ZS, JMD, LAC, WCF; Investigation, KEW, JAS, SG, JE, GK, BJP, RGA, DR, BCT, AA, MP; Writing-Original Draft, KEW, JAS, AJA; Visualization, MUS, JAS, KEW; Resources, JAS, AJA, KEW, JF, SRP, TZ, SG, JMD

Declaration of Interests

AJA receives consulting income and research support to Duke from Pfizer/Astellas, Bayer, Dendreon, Merck, AstraZeneca, and Janssen. He receives research support to Duke from BMS, Constellation, Gilead, Genentech/Roche. MP and EP are inventors on

US Government and University assigned patents and patent applications that cover aspects of the technologies discussed such as Reverse Phase Protein Microarrays. As inventors, they are entitled to receive royalties as provided by US Law and George Mason University policy. MP and EP receive royalties from Avant Diagnostics. EP is consultant to and shareholder of Avant Diagnostics, Inc and Perthera, Inc. All other authors declare no competing interests.

Figure Titles and Legends

Figure 1

Model of ecological responses to loss of AR signaling. Adaptation to enzalutamide centers around three phenotypes: 1) Pro-survival stress response; 2) Immune evasion; and 3) Metastasis.

Figure 2

Enzalutamide resistant cell lines retain AR expression and do not undergo a NEPC/EMT/Stem transition. A. Development of enzalutamide resistant cell lines. **B.** Control (ctrl) and enzaR cell lines were treated for 10 days with vehicle (DMSO) or two doses of enzalutamide (25μM or 50μM), and cell growth and apoptosis were measured. *= $p<0.05$; student's t-test. Error bars represent the standard error of the mean. **C-D.** AR-FL and AR-V7 mRNA (**C**) and protein expression (**D**) measured by qRT-PCR and western blot, respectively, *$p<0.05$; student's t-test. Mean cell values are plotted along with standard error of the mean. **E.** Summary table characterizing the diversity of known

457 resistance mechanisms in enzalutamide resistant cell lines. ADT, androgen deprivation
458 therapy; Enza, enzalutamide; EnzaR, enzalutamide resistant.
459
460 **Figure 3**
461 **Diverse gene expression during enzalutamide resistance converges on activation of**
462 **stress response MAPK p38. A.** Venn diagrams representing common gene expression
463 alterations by RNA-Seq or protein activation by proteomics analysis (top). Enriched
464 pathways in each matched enzaR cell line using gene set enrichment analysis (bottom)
465 from RNA-Seq data. **B.** Combined RNA-Seq analysis from all enzalutamide-resistant
466 lines identified p38/MAPK signaling and stress-related pathways. **C.** Volcano plot
467 representing changes in phosphorylation from reverse phase protein array analysis. **D.**
468 RNA-Seq analysis for pathway enrichment scores in MDA-PCa-2b cells. **E.** Western blot
469 analysis of phosph-p38 in MDA-PCa-2b cells. **F.** Immunohistochemical staining of
470 phospho-p38 is strongly enriched in metastatic tissues compared to localized samples.
471 Representative images show phospho-p38 staining in localized and metastatic prostate
472 cancer tissues. **G.** Kinase substrate enrichment analysis (KSEA) of p-p38 revealed an
473 enrichment of p38 substrates in metastatic CRPC patients using published
474 phosphoproteomic datasets.
475
476 **Figure 4**
477 **p38 inhibition is important for cell growth in EnzaR cell lines. A-C.** Control or enzaR
478 cells were cultured in media containing DMSO or 25μM SB203580, and cell confluence
479 was quantified using the IncuCyte basic analyzer. **D-F.** Control or enzaR cells, treated

480 with androgen (R1881), p38 inhibitor (SB203580), or the combination of R1881 and
481 SB203580 were analyzed for PSA mRNA expression. Amounts were determined by
482 qRT-PCR and normalized to GAPDH, * = $p<0.05$; student's t-test.
483
484 **Figure 5**
485 **Molecular alteration of p38 expression regulates enzalutamide sensitivity. A.** EnzaR
486 cells with p38 knockout were cultured and cell confluence was quantified using the
487 IncuCyte basic analyzer. Knockout of p38 in enzaR cell line populations decreases cell
488 proliferation of LNCaP (A) and LN95 cells (B). **C.D.** Enzalutamide sensitive cells
489 engineered to overexpress p38 were cultured and cell confluence was quantified as
490 above. Overexpression of p38α in enzalutamide sensitive control cell lines increases cell
491 growth in response to enzalutamide treatment. **E.** Mice were injected subcutaneously
492 with 8 x 10^6 CS2-enzaR cells and treated with diluent or 15 mg/kg of p38 inhibitor
493 (SB203580). Tumor growth was measured weakly over 13 weeks. * = $p<0.05$; student's
494 t-test. **F.** Representative 10X images of H&E staining from xenograft tumors collected
495 after treatment with diluent or p38 inhibitor (15 mg/kg SB203580) demonstrating viable
496 (top) and necrotic (bottom) tumor.
497
498 **Figure 6**
499 **PD-L1 expression correlates with Snail expression and activity during enzalutamide**
500 **resistance. A.** Western blot analysis of phospho-p38 and Snail expression in control and
501 enzaR cell lines. GAPDH is used as a loading control. **B.** Analysis of RNA-Seq data from
502 The Cancer Genome Atlas reveals a significant positive correlation between Snail and

PD-L1 expression in prostate cancer tissues. **C.** PD-L1 mRNA expression in LN95 cells with and without Snail activation. **D.** Snail and PD-L1 protein expression in LN95 cells with and without Snail activation. Blue: Hoechst stained nuclei; Red stained Snail; Green stained PD-L1.

Figure 7

p38 is a druggable target upstream of Snail and PD-L1. A. PD-L1 protein expression is significantly increased in enzaR cells by reverse phase protein array analysis. **B-C.** PD-L1 mRNA (**B**) and protein (**C**) expression measured by qPCR and western blot, respectively, in enzaR cells. **D.** Western blot analysis of p38, Snail, and PD-L1 in LN95 enzaR cells with p38α knockout. NaKATPase is used as a loading control. **E.** Western blot analysis of p38, Snail, and PD-L1 in LN95 control cells with p38α activation. NaKATPase is used as a loading control. **F.** Model of p38 as a druggable target upstream of Snail and PD-L1 induced during resistance to enzalutamide.

Materials and Methods

Patient samples

For metastatic prostate cancer samples (n=20) and a second cohort of localized prostate cancer samples (n=30), formalin fixed metastatic tissue was collected from the Duke University pathology department and Duke Cancer Institute Biorepository Core under a separate Duke IRB approved protocol. Clinical data on prior therapy and metastatic site were collected.

526 **Cell lines**

527 MDA-PCa-2b and LNCaP cells were obtained from ATCC using the Duke University
528 Cell Culture Facility. MDA-PCa-2b cells were cultured in F12-K media supplemented
529 with 20% fetal bovine serum (Sigma), 1% penicillin/streptomycin streptomycin (Life
530 Technologies), cholera toxin, epidermal growth factor, phosphoethanolamine,
531 hydrocortisone, sodium selenite, and insulin as recommended by ATCC. LNCaP cells
532 were cultured in RPMI containing 10% fetal bovine serum and 1%
533 penicillin/streptomycin. LNCaP95 cells were kindly provided by Dr. Scott Dehm
534 (University of Minnesota) and are reported in previous studies (Liu et al., 2013; Ware et
535 al., 2016). LNCaP95 and CS2 cells are androgen-independent cell lines derived from the
536 parental LNCaP cells. LNCaP95 and CS2 were cultured in RPMI containing 10%
537 charcoal stripped fetal bovine serum and 1% penicillin/streptomycin. Resistant cell
538 populations were cultured with the addition of 50 μM enzalutamide (provided by
539 Medivation/Astellas). Enzalutamide resistant cells (EnzaR cells) were generated by
540 chronic culture with increasing doses of enzalutamide to a concentration of 50 μM. Cells
541 were authenticated and re-authenticated following enzalutamide resistant through
542 sequencing including the presence of known LNCaP AR ligand binding domain mutation
543 T877A. Cells stably expressing inducible Snail (Addgene plasmid #18798), constitutively
544 active p38 or MAPK14 gRNA targets were generated by transduction of cells as
545 described previously (Mani et al., 2008).
546
547
548

549 **Cell growth and viability assays**

550 Control and Enza-R cells were cultured in media containing DMSO (Sigma) or 50 μM
551 enzalutamide for at least one week. Cells were counted using the Countess II (Life
552 Technologies), 2500 cells were seeded in a 96-well plate. Cell confluence was monitored
553 using the IncuCyte live cell analysis system (Essen Biosciences) and standard error of the
554 mean (SEM) was calculated from triplicate wells. For cells stably expressing p38 or
555 MAPK14 gRNA, cells were treated with DMSO or 25 μM of SB203580 (selleckchem)
556 and monitored as above. For cell viability, apoptosis was measured after 10 days of drug
557 treatment using the IncuCyte Caspase-3/7 green apoptosis assay reagent and quantified
558 using the IncuCyte basic analyzer.
559
560 **RNA-seq**
561 Total RNA was isolated using the Quick-RNA Miniprep kit (Zymo Research). RNA-seq,
562 total RNA was submitted to the Duke Center for Genomic and Computational Biology
563 core for sample preparation, sequencing, and analysis. RNA-seq data was processed
564 using the TrimGalore toolkit
565 (http://www.bioinformatics.babraham.ac.uk/projects/trim_galore) which employs
566 Cutadapt[1] to trim low quality bases and Illumina sequencing adapters from the 3' end of
567 the reads. Only pairs where both reads were 20nt or longer were kept for further analysis.
568 Reads were mapped to the GRCh37v73 version of the human genome and transcriptome[2]
569 using the STAR RNA-seq alignment tool[3]. Reads were kept for subsequent analysis if
570 they mapped to a single genomic location. Gene counts were compiled using the HTSeq
571 tool (http://www-huber.embl.de/users/anders/HTSeq/). Only genes that had at least 40

572 reads in any given library were used in subsequent analysis. Normalization and
573 differential expression was carried out using the EdgeR[4] Bioconductor[5] package with the
574 R statistical programming environment (www.r-project.org). A negative binomial
575 generalized log-linear model[6] was used to identify differentially expressed genes between
576 the different genotypes when comparing against specific control samples. Enriched
577 pathways were determined by GSEA[7] for each comparison.
578
579 **Real-Time quantitative RT-PCR**
580 For qPCR, total RNA was reverse transcribed using the High-Capacity cDNA Reverse
581 Transcription Kit (Life Technologies). Aliquots of 5-fold diluted reverse transcription
582 reactions were subjected to quantitative (q)PCR with KAPA SYBR FAST master mix
583 using the Vii7 real time-PCR detection system (Applied Biosystems). GAPDH mRNA
584 levels were measured for normalization, and the data are presented as "Relative
585 Expression". A complete list of primer sequences is provided in the supplementary text.
586
587 **TCGA Analysis**
588 The results published here are in part based upon data generated by The Cancer Genome
589 Atlas (TCGA) Research Network: http://cancergenome.nih.gov. Data available from
590 TCGA was analyzed using the Kruskal Wallis test to evaluate the correlation between
591 Snail expression and PD-L1 expression from prostate cancer patients.
592
593
594

Reverse phase protein array

Cells were seeded (300,000/well) in 6-well plates and allowed to incubate for 5 days. Cells were then rinsed with PBS, flash frozen, and analyzed as previously described (Baldelli et al., 2017; Pierobon et al., 2017).

Immunoblot analyses

For immunoblot analysis cells extracts were mixed with SDS sample buffer and submitted to SDS-PAGE. Following electrophoretic transfer onto nitrocellulose, the filters were blocked in Starting Block (Thermo), incubated with antibodies and developed using the Odyssey-FC imager (LI-COR).

A complete list of primary antibodies and their dilutions is provided in the supplementary text.

Immunofluorescence staining

For cells expressing inducible Snail, cells were pretreated with ethanol (EtOH) or 4OHT. For immunofluorescence (IF) staining, cells were fixed in 4% PFA, permeabilized with 0.2% Triton X-100, and stained with Hoechst. Cells were blocked with 5% bovine serum albumin (BSA, Sigma) prior to incubation with primary antibodies. Cells were incubated in Alexa Fluor secondary antibodies (Life Technologies) and then imaged on an inverted Olympus IX 73 epifluorescence microscope.

Immunohistochemistry

We performed antibody optimization and analytic validation for all antibodies as previously described (Armstrong et al., 2016). An expert prostate cancer pathologist blinded to outcomes evaluated antibody staining in parallel with hematoxylin and eosin. Scoring of each biomarker used a 0 to 3 scale for both intensity and a <25%, <50%, <75%, <100% scale for frequency of expression in each tumor sample.

Animal Experiments

Six to eight week male mice were injected subcutaneously with 8 x 10^6 CS2-enzaR cells. Prior to injection cells were resuspended in 50% matrigel supplemented with 10%FBS/RPMI. Mice were treated with diluent or 15 mg/kg of p38 inhibitor (SB203580). Tumor growth was measured using calipers weakly over 13 weeks.

Statistical Analysis

Data are shown as means ± SEM. Student's t-test or multiple group comparison was performed by one-way ANOVA followed by the Sidak method for comparison of means. $P \leq 0.05$ is considered significant. Differences in phospho-p38 expression between localized and metastatic samples were analyzed using a Chi-square test. Data available through the TCGA was analyzed using the Kruskal Wallis test using JMP (version pro 12). All other analyses were performed using Prism (version 8.0d).

641 **Supplemental Information Titles and Legends**

642 **Figure 1**

643 **Treatment with enzalutamide enriches for the F876L agonist mutation in LNCaP**

644 **enzaR cells.** Alignment of RNA-seq tracks using the integrative genomic viewer.

645

646 **Figure 2**

647 **Copy number alterations in control versus enzaR cell lines.** Array comparative

648 genomic hybridization from genomic DNA isolated from paired enzaR cell line models.

649 Alteration losses and gains greater than one log are highlighted in blue or red,

650 respectively.

651

652 **Figure 3**

653 **EnzaR cell lines do not undergo NEPC/Stemness transitions. A.** Representative

654 images of enzalutamide sensitive and resistant cell lines. **B.** qPCR expression analysis of

655 driver genes involved in neuroendocrine and stem cell pathways.

656

657 **Figure 4**

658 **Copy number alterations do not converge between enzaR cell lines.** Venn diagrams

659 comparing copy number gains and losses between control and enzaR cell lines.

660

661 **Figure 5**

662 **EnzaR cell lines acquire very few nucleotide variants during adaptation to**

663 **enzalutamide. A.** Venn diagrams comparing nucleotide variants between paired control

664 and enzaR cell lines. **B.** Venn diagram comparing common nucleotide variants observed
665 in enzaR compared to control cell lines.
666
667 **Figure 6**
668 **AR activity is inhibited by p38 inhibition. A.** Control or enzaR cells, treated with
669 androgen (R1881), p38 inhibitor (SB203580), or the combination of R1881 and
670 SB203580 were analyzed for NKX3.1 mRNA expression. Amounts were determined by
671 qRT-PCR and normalized to GAPDH. **B.** Western blot analysis of phospho-p38
672 expression in control and enzaR cell lines with acute enzalutamide (10 μM) treatment.
673
674 **Figure 7**
675 **EnzaR cells display markers of a dormant phenotype. A.** Ratios of phospho-ERK to
676 phospho-p38 protein levels. **B.** Western blot analysis of p21 expression in control and
677 enzaR cell line models. **C.** Beta-galactosidase activity in response to enzalutamide
678 treatment in LNCaP cells.
679
680 **Figure 8**
681 **Molecular alteration of p38 expression regulates enzalutamide sensitivity. A.** GSK3β
682 serine 9 phosphorylation is significantly increased in enzaR cells by reverse phase protein
683 array analysis.
684

References

Akbani, R., Becker, K. F., Carragher, N., Goldstein, T., de Koning, L., Korf, U., Liotta, L., Mills, G. B., Nishizuka, S. S., Pawlak, M., *et al.* (2014). Realizing the promise of reverse phase protein arrays for clinical, translational, and basic research: a workshop report: the RPPA (Reverse Phase Protein Array) society. Molecular & cellular proteomics : MCP *13*, 1625-1643.

Antonarakis, E. S., Lu, C., Wang, H., Luber, B., Nakazawa, M., Roeser, J. C., Chen, Y., Mohammad, T. A., Chen, Y., Fedor, H. L., *et al.* (2014). AR-V7 and resistance to enzalutamide and abiraterone in prostate cancer. The New England journal of medicine *371*, 1028-1038.

Antonarakis, E. S., Piulats, J. M., Gross-Goupil, M., Goh, J., Ojamaa, K., Hoimes, C. J., Vaishampayan, U., Berger, R., Sezer, A., Alanko, T., *et al.* (2020). Pembrolizumab for Treatment-Refractory Metastatic Castration-Resistant Prostate Cancer: Multicohort, Open-Label Phase II KEYNOTE-199 Study. Journal of clinical oncology : official journal of the American Society of Clinical Oncology *38*, 395-405.

Aparicio, A., Tzelepi, V., Araujo, J. C., Guo, C. C., Liang, S., Troncoso, P., Logothetis, C. J., Navone, N. M., and Maity, S. N. (2011). Neuroendocrine prostate cancer xenografts with large-cell and small-cell features derived from a single patient's tumor: morphological, immunohistochemical, and gene expression profiles. The Prostate *71*, 846-856.

Armstrong, A. J., Healy, P., Halabi, S., Vollmer, R., Lark, A., Kemeny, G., Ware, K., and Freedland, S. J. (2016). Evaluation of an epithelial plasticity biomarker panel in men with localized prostate cancer. Prostate cancer and prostatic diseases *19*, 40-45.

Arora, V. K., Schenkein, E., Murali, R., Subudhi, S. K., Wongvipat, J., Balbas, M. D., Shah, N., Cai, L., Efstathiou, E., Logothetis, C., *et al.* (2013). Glucocorticoid receptor confers resistance to antiandrogens by bypassing androgen receptor blockade. Cell *155*, 1309-1322.

Azad, A. A., Volik, S. V., Wyatt, A. W., Haegert, A., Le Bihan, S., Bell, R. H., Anderson, S. A., McConeghy, B., Shukin, R., Bazov, J., *et al.* (2015). Androgen Receptor Gene Aberrations in Circulating Cell-Free DNA: Biomarkers of Therapeutic Resistance in Castration-Resistant Prostate Cancer. Clinical cancer research : an official journal of the American Association for Cancer Research *21*, 2315-2324.

Balbas, M. D., Evans, M. J., Hosfield, D. J., Wongvipat, J., Arora, V. K., Watson, P. A., Chen, Y., Greene, G. L., Shen, Y., and Sawyers, C. L. (2013). Overcoming mutation-based resistance to antiandrogens with rational drug design. eLife *2*, e00499.

Baldelli, E., Calvert, V., Hodge, A., VanMeter, A., Petricoin, E. F., 3rd, and Pierobon, M. (2017). Reverse Phase Protein Microarrays. Methods in molecular biology *1606*, 149-169.

Beer, T. M., Armstrong, A. J., Rathkopf, D. E., Loriot, Y., Sternberg, C. N., Higano, C. S., Iversen, P., Bhattacharya, S., Carles, J., Chowdhury, S., *et al.* (2014). Enzalutamide in metastatic prostate cancer before chemotherapy. The New England journal of medicine *371*, 424-433.

Bikkavilli, R. K., Feigin, M. E., and Malbon, C. C. (2008). p38 mitogen-activated protein kinase regulates canonical Wnt-beta-catenin signaling by inactivation of GSK3beta. Journal of cell science *121*, 3598-3607.

731 Bishop, J. L., Sio, A., Angeles, A., Roberts, M. E., Azad, A. A., Chi, K. N., and Zoubeidi, A.
732 (2015). PD-L1 is highly expressed in Enzalutamide resistant prostate cancer.
733 Oncotarget *6*, 234-242.
734 Bluemn, E. G., Coleman, I. M., Lucas, J. M., Coleman, R. T., Hernandez-Lopez, S.,
735 Tharakan, R., Bianchi-Frias, D., Dumpit, R. F., Kaipainen, A., Corella, A. N., *et al.*
736 (2017). Androgen Receptor Pathway-Independent Prostate Cancer Is Sustained
737 through FGF Signaling. Cancer cell *32*, 474-489 e476.
738 Bryce, A. H., Alumkal, J. J., Armstrong, A., Higano, C. S., Iversen, P., Sternberg, C. N.,
739 Rathkopf, D., Loriot, Y., de Bono, J., Tombal, B., *et al.* (2017). Radiographic
740 progression with nonrising PSA in metastatic castration-resistant prostate cancer:
741 post hoc analysis of PREVAIL. Prostate cancer and prostatic diseases *20*, 221-227.
742 Canovas, B., Igea, A., Sartori, A. A., Gomis, R. R., Paull, T. T., Isoda, M., Perez-Montoyo,
743 H., Serra, V., Gonzalez-Suarez, E., Stracker, T. H., and Nebreda, A. R. (2018). Targeting
744 p38alpha Increases DNA Damage, Chromosome Instability, and the Anti-tumoral
745 Response to Taxanes in Breast Cancer Cells. Cancer cell *33*, 1094-1110 e1098.
746 Chakraborty, G., Armenia, J., Mazzu, Y. Z., Nandakumar, S., Stopsack, K. H., Atiq, M. O.,
747 Komura, K., Jehane, L., Hirani, R., Chadalavada, K., *et al.* (2019). Significance of
748 BRCA2 and RB1 Co-loss in Aggressive Prostate Cancer Progression. Clinical cancer
749 research : an official journal of the American Association for Cancer Research.
750 Chen, C. D., Welsbie, D. S., Tran, C., Baek, S. H., Chen, R., Vessella, R., Rosenfeld, M. G.,
751 and Sawyers, C. L. (2004). Molecular determinants of resistance to antiandrogen
752 therapy. Nature medicine *10*, 33-39.
753 Chen, M., and Xie, S. (2018). Therapeutic targeting of cellular stress responses in
754 cancer. Thoracic cancer *9*, 1575-1582.
755 Chen, X. H., Liu, Z. C., Zhang, G., Wei, W., Wang, X. X., Wang, H., Ke, H. P., Zhang, F.,
756 Wang, H. S., Cai, S. H., and Du, J. (2015). TGF-beta and EGF induced HLA-I
757 downregulation is associated with epithelial-mesenchymal transition (EMT)
758 through upregulation of snail in prostate cancer cells. Molecular immunology *65*, 34-
759 42.
760 Chen, Y., Wang, L., Jin, J., Luan, Y., Chen, C., Li, Y., Chu, H., Wang, X., Liao, G., Yu, Y., *et*
761 *al.* (2017). p38 inhibition provides anti-DNA virus immunity by regulation of USP21
762 phosphorylation and STING activation. The Journal of experimental medicine *214*,
763 991-1010.
764 Chery, L., Lam, H. M., Coleman, I., Lakely, B., Coleman, R., Larson, S., Aguirre-Ghiso, J.
765 A., Xia, J., Gulati, R., Nelson, P. S., *et al.* (2014). Characterization of single
766 disseminated prostate cancer cells reveals tumor cell heterogeneity and identifies
767 dormancy associated pathways. Oncotarget *5*, 9939-9951.
768 Coulthard, L. R., White, D. E., Jones, D. L., McDermott, M. F., and Burchill, S. A. (2009).
769 p38(MAPK): stress responses from molecular mechanisms to therapeutics. Trends
770 in molecular medicine *15*, 369-379.
771 Dardenne, E., Beltran, H., Benelli, M., Gayvert, K., Berger, A., Puca, L., Cyrta, J., Sboner,
772 A., Noorzad, Z., MacDonald, T., *et al.* (2016). N-Myc Induces an EZH2-Mediated
773 Transcriptional Program Driving Neuroendocrine Prostate Cancer. Cancer cell *30*,
774 563-577.

de Bono, J. S., Logothetis, C. J., Molina, A., Fizazi, K., North, S., Chu, L., Chi, K. N., Jones, R. J., Goodman, O. B., Jr., Saad, F., *et al.* (2011). Abiraterone and increased survival in metastatic prostate cancer. The New England journal of medicine *364*, 1995-2005.

Decker, A. M., Jung, Y., Cackowski, F. C., Yumoto, K., Wang, J., and Taichman, R. S. (2017). Sympathetic Signaling Reactivates Quiescent Disseminated Prostate Cancer Cells in the Bone Marrow. Molecular cancer research : MCR *15*, 1644-1655.

Drake, J. M., Paull, E. O., Graham, N. A., Lee, J. K., Smith, B. A., Titz, B., Stoyanova, T., Faltermeier, C. M., Uzunangelov, V., Carlin, D. E., *et al.* (2016). Phosphoproteome Integration Reveals Patient-Specific Networks in Prostate Cancer. Cell *166*, 1041-1054.

Flem-Karlsen, K., Tekle, C., Oyjord, T., Florenes, V. A., Maelandsmo, G. M., Fodstad, O., and Nunes-Xavier, C. E. (2019). p38 MAPK activation through B7-H3-mediated DUSP10 repression promotes chemoresistance. Scientific reports *9*, 5839.

Gao, J., Ward, J. F., Pettaway, C. A., Shi, L. Z., Subudhi, S. K., Vence, L. M., Zhao, H., Chen, J., Chen, H., Efstathiou, E., *et al.* (2017). VISTA is an inhibitory immune checkpoint that is increased after ipilimumab therapy in patients with prostate cancer. Nature medicine *23*, 551-555.

Gatenby, R. A., Gillies, R. J., and Brown, J. S. (2011). Of cancer and cave fish. Nature reviews Cancer *11*, 237-238.

Goodwin, J. F., Kothari, V., Drake, J. M., Zhao, S., Dylgjeri, E., Dean, J. L., Schiewer, M. J., McNair, C., Jones, J. K., Aytes, A., *et al.* (2015). DNA-PKcs-Mediated Transcriptional Regulation Drives Prostate Cancer Progression and Metastasis. Cancer cell *28*, 97-113.

Graff, J. N., Alumkal, J. J., Drake, C. G., Thomas, G. V., Redmond, W. L., Farhad, M., Cetnar, J. P., Ey, F. S., Bergan, R. C., Slottke, R., and Beer, T. M. (2016). Early evidence of anti-PD-1 activity in enzalutamide-resistant prostate cancer. Oncotarget *7*, 52810-52817.

Graff, J. N., Alumkal, J. J., Thompson, R. F., Moran, A., Thomas, G. V., Wood, M. A., Drake, C. G., Slottke, R., and Beer, T. M. (2018). Pembrolizumab (Pembro) plus enzalutamide (Enz) in metastatic castration resistant prostate cancer (mCRPC): Extended follow up. Journal of Clinical Oncology *36*, 5047-5047.

Harrison, J. C., Zyla, T. R., Bardes, E. S., and Lew, D. J. (2004). Stress-specific activation mechanisms for the "cell integrity" MAPK pathway. The Journal of biological chemistry *279*, 2616-2622.

Hu, R., Lu, C., Mostaghel, E. A., Yegnasubramanian, S., Gurel, M., Tannahill, C., Edwards, J., Isaacs, W. B., Nelson, P. S., Bluemn, E., *et al.* (2012). Distinct transcriptional programs mediated by the ligand-dependent full-length androgen receptor and its splice variants in castration-resistant prostate cancer. Cancer research *72*, 3457-3462.

Igea, A., and Nebreda, A. R. (2015). The Stress Kinase p38alpha as a Target for Cancer Therapy. Cancer research *75*, 3997-4002.

Khandrika, L., Lieberman, R., Koul, S., Kumar, B., Maroni, P., Chandhoke, R., Meacham, R. B., and Koul, H. K. (2009). Hypoxia-associated p38 mitogen-activated protein kinase-mediated androgen receptor activation and increased HIF-1alpha levels contribute to emergence of an aggressive phenotype in prostate cancer. Oncogene *28*, 1248-1260.

Kllduff, T. S. (2004). Hibernation. Encyclopedia of Neuroscience, 1113-1117.
Kim, S., Koh, J., Kim, M. Y., Kwon, D., Go, H., Kim, Y. A., Jeon, Y. K., and Chung, D. H. (2016). PD-L1 expression is associated with epithelial-to-mesenchymal transition in adenocarcinoma of the lung. Human pathology *58*, 7-14.
Korpal, M., Korn, J. M., Gao, X., Rakiec, D. P., Ruddy, D. A., Doshi, S., Yuan, J., Kovats, S. G., Kim, S., Cooke, V. G., *et al.* (2013). An F876L mutation in androgen receptor confers genetic and phenotypic resistance to MDV3100 (enzalutamide). Cancer Discov *3*, 1030-1043.
Koul, H. K., Pal, M., and Koul, S. (2013). Role of p38 MAP Kinase Signal Transduction in Solid Tumors. Genes & cancer *4*, 342-359.
Ku, S. Y., Rosario, S., Wang, Y., Mu, P., Seshadri, M., Goodrich, Z. W., Goodrich, M. M., Labbe, D. P., Gomez, E. C., Wang, J., *et al.* (2017). Rb1 and Trp53 cooperate to suppress prostate cancer lineage plasticity, metastasis, and antiandrogen resistance. Science *355*, 78-83.
Lehuede, C., Dupuy, F., Rabinovitch, R., Jones, R. G., and Siegel, P. M. (2016). Metabolic Plasticity as a Determinant of Tumor Growth and Metastasis. Cancer research *76*, 5201-5208.
Li, M., Liu, J., and Zhang, C. (2011a). Evolutionary history of the vertebrate mitogen activated protein kinases family. PloS one *6*, e26999.
Li, Y., Alsagabi, M., Fan, D., Bova, G. S., Tewfik, A. H., and Dehm, S. M. (2011b). Intragenic rearrangement and altered RNA splicing of the androgen receptor in a cell-based model of prostate cancer progression. Cancer research *71*, 2108-2117.
Li, Y., Hwang, T. H., Oseth, L. A., Hauge, A., Vessella, R. L., Schmechel, S. C., Hirsch, B., Beckman, K. B., Silverstein, K. A., and Dehm, S. M. (2012). AR intragenic deletions linked to androgen receptor splice variant expression and activity in models of prostate cancer progression. Oncogene *31*, 4759-4767.
Liu, C. L., Chen, S. F., Wu, M. Z., Jao, S. W., Lin, Y. S., Yang, C. Y., Lee, T. Y., Wen, L. W., Lan, G. L., and Nieh, S. (2016). The molecular and clinical verification of therapeutic resistance via the p38 MAPK-Hsp27 axis in lung cancer. Oncotarget *7*, 14279-14290.
Liu, G., Sprenger, C., Sun, S., Epilepsia, K. S., Haugk, K., Zhang, X., Coleman, I., Nelson, P. S., and Plymate, S. (2013). AR variant ARv567es induces carcinogenesis in a novel transgenic mouse model of prostate cancer. Neoplasia *15*, 1009-1017.
Liu, L. L., Xie, N., Sun, S., Plymate, S., Mostaghel, E., and Dong, X. (2014). Mechanisms of the androgen receptor splicing in prostate cancer cells. Oncogene *33*, 3140-3150.
Lu, H., Tran, L., Park, Y., Chen, I., Lan, J., Xie, Y., and Semenza, G. L. (2018). Reciprocal Regulation of DUSP9 and DUSP16 Expression by HIF1 Controls ERK and p38 MAP Kinase Activity and Mediates Chemotherapy-Induced Breast Cancer Stem Cell Enrichment. Cancer research *78*, 4191-4202.
Mani, S. A., Guo, W., Liao, M. J., Eaton, E. N., Ayyanan, A., Zhou, A. Y., Brooks, M., Reinhard, F., Zhang, C. C., Shipitsin, M., *et al.* (2008). The epithelial-mesenchymal transition generates cells with properties of stem cells. Cell *133*, 704-715.
Mazrooei, P., Kron, K. J., Zhu, Y., Zhou, S., Grillo, G., Mehdi, T., Ahmed, M., Severson, T. M., Guilhamon, P., Armstrong, N. S., *et al.* (2019). Cistrome Partitioning Reveals Convergence of Somatic Mutations and Risk Variants on Master Transcription Regulators in Primary Prostate Tumors. Cancer cell *36*, 674-689 e676.

Medici, D., Potenta, S., and Kalluri, R. (2011). Transforming growth factor-beta2 promotes Snail-mediated endothelial-mesenchymal transition through convergence of Smad-dependent and Smad-independent signalling. The Biochemical journal *437*, 515-520.

Miao, L., Yang, L., Li, R., Rodrigues, D. N., Crespo, M., Hsieh, J. T., Tilley, W. D., de Bono, J., Selth, L. A., and Raj, G. V. (2017). Disrupting Androgen Receptor Signaling Induces Snail-Mediated Epithelial-Mesenchymal Plasticity in Prostate Cancer. Cancer research *77*, 3101-3112.

Mills, I. G. (2014). Maintaining and reprogramming genomic androgen receptor activity in prostate cancer. Nature reviews Cancer *14*, 187-198.

Mu, P., Zhang, Z., Benelli, M., Karthaus, W. R., Hoover, E., Chen, C. C., Wongvipat, J., Ku, S. Y., Gao, D., Cao, Z., *et al.* (2017). SOX2 promotes lineage plasticity and antiandrogen resistance in TP53- and RB1-deficient prostate cancer. Science *355*, 84-88.

Noh, H., Hu, J., Wang, X., Xia, X., Satelli, A., and Li, S. (2015). Immune checkpoint regulator PD-L1 expression on tumor cells by contacting CD11b positive bone marrow derived stromal cells. Cell communication and signaling : CCS *13*, 14.

Paranjape, A. N., Soundararajan, R., Werden, S. J., Joseph, R., Taube, J. H., Liu, H., Rodriguez-Canales, J., Sphyris, N., Wistuba, I., Miura, N., *et al.* (2016). Inhibition of FOXC2 restores epithelial phenotype and drug sensitivity in prostate cancer cells with stem-cell properties. Oncogene *35*, 5963-5976.

Penson, D. F., Armstrong, A. J., Concepcion, R., Agarwal, N., Olsson, C., Karsh, L., Dunshee, C., Wang, F., Wu, K., Krivoshik, A., *et al.* (2016). Enzalutamide Versus Bicalutamide in Castration-Resistant Prostate Cancer: The STRIVE Trial. Journal of clinical oncology : official journal of the American Society of Clinical Oncology *34*, 2098-2106.

Pierobon, M., Ramos, C., Wong, S., Hodge, K. A., Aldrich, J., Byron, S., Anthony, S. P., Robert, N. J., Northfelt, D. W., Jahanzeb, M., *et al.* (2017). Enrichment of PI3K-AKT-mTOR Pathway Activation in Hepatic Metastases from Breast Cancer. Clinical cancer research : an official journal of the American Association for Cancer Research *23*, 4919-4928.

Robinson, D., Van Allen, E. M., Wu, Y. M., Schultz, N., Lonigro, R. J., Mosquera, J. M., Montgomery, B., Taplin, M. E., Pritchard, C. C., Attard, G., *et al.* (2015). Integrative Clinical Genomics of Advanced Prostate Cancer. Cell *162*, 454.

Romanel, A., Tandefelt, D. G., Conteduca, V., Jayaram, A., Casiraghi, N., Wetterskog, D., Salvi, S., Amadori, D., Zafeiriou, Z., Rescigno, P., *et al.* (2015). Plasma AR and abiraterone-resistant prostate cancer. Sci Transl Med *7*, 312re310.

Ruppender, N. S., Morrissey, C., Lange, P. H., and Vessella, R. L. (2013). Dormancy in solid tumors: implications for prostate cancer. Cancer metastasis reviews *32*, 501-509.

Ryan, C. J., Smith, M. R., de Bono, J. S., Molina, A., Logothetis, C. J., de Souza, P., Fizazi, K., Mainwaring, P., Piulats, J. M., Ng, S., *et al.* (2013). Abiraterone in metastatic prostate cancer without previous chemotherapy. The New England journal of medicine *368*, 138-148.

Ryu, K. J., Park, S. M., Park, S. H., Kim, I. K., Han, H. T., Kim, H. J., Kim, S. H., Hong, K. S., Kim, H., Kim, M., *et al.* (2019). p38 Stabilizes Snail by Suppressing DYRK2-Mediated

912 Phosphorylation that is Required for GSK3beta-betaTrCP-Induced Snail
913 Degradation. Cancer research.
914 Scher, H. I., Beer, T. M., Higano, C. S., Anand, A., Taplin, M. E., Efstathiou, E., Rathkopf,
915 D., Shelkey, J., Yu, E. Y., Alumkal, J., *et al.* (2010). Antitumour activity of MDV3100 in
916 castration-resistant prostate cancer: a phase 1-2 study. Lancet *375*, 1437-1446.
917 Scher, H. I., Fizazi, K., Saad, F., Taplin, M. E., Sternberg, C. N., Miller, K., de Wit, R.,
918 Mulders, P., Chi, K. N., Shore, N. D., *et al.* (2012). Increased survival with
919 enzalutamide in prostate cancer after chemotherapy. The New England journal of
920 medicine *367*, 1187-1197.
921 Skov, C., Aarestrup, K., Baktoft, H., Brodersen, J., Brönmark, C., Hansson, L.-A.,
922 Nielsen, E. E., Nielsen, T., and Nilsson, P. A. (2010). Influences of environmental cues,
923 migration history, and habitat familiarity on partial migration. Behavioral Ecology
924 *21*, 1140-1146.
925 Sosa, M. S., Avivar-Valderas, A., Bragado, P., Wen, H. C., and Aguirre-Ghiso, J. A.
926 (2011). ERK1/2 and p38alpha/beta signaling in tumor cell quiescence:
927 opportunities to control dormant residual disease. Clinical cancer research : an
928 official journal of the American Association for Cancer Research *17*, 5850-5857.
929 Sun, S., and Zhou, J. (2018). Molecular mechanisms underlying stress response and
930 adaptation. Thoracic cancer *9*, 218-227.
931 Thornton, T. M., Pedraza-Alva, G., Deng, B., Wood, C. D., Aronshtam, A., Clements, J. L.,
932 Sabio, G., Davis, R. J., Matthews, D. E., Doble, B., and Rincon, M. (2008).
933 Phosphorylation by p38 MAPK as an alternative pathway for GSK3beta inactivation.
934 Science *320*, 667-670.
935 Tran, C., Ouk, S., Clegg, N. J., Chen, Y., Watson, P. A., Arora, V., Wongvipat, J., Smith-
936 Jones, P. M., Yoo, D., Kwon, A., *et al.* (2009). Development of a second-generation
937 antiandrogen for treatment of advanced prostate cancer. Science *324*, 787-790.
938 van der Toom, E. E., Verdone, J. E., and Pienta, K. J. (2016). Disseminated tumor cells
939 and dormancy in prostate cancer metastasis. Current opinion in biotechnology *40*,
940 9-15.
941 Varpe, O. (2017). Life History Adaptations to Seasonality. Integrative and
942 comparative biology *57*, 943-960.
943 Viswanathan, S. R., Ha, G., Hoff, A. M., Wala, J. A., Carrot-Zhang, J., Whelan, C. W.,
944 Haradhvala, N. J., Freeman, S. S., Reed, S. C., Rhoades, J., *et al.* (2018). Structural
945 Alterations Driving Castration-Resistant Prostate Cancer Revealed by Linked-Read
946 Genome Sequencing. Cell *174*, 433-447 e419.
947 Wang, S., Yang, J., Qian, J., Wezeman, M., Kwak, L. W., and Yi, Q. (2006). Tumor
948 evasion of the immune system: inhibiting p38 MAPK signaling restores the function
949 of dendritic cells in multiple myeloma. Blood *107*, 2432-2439.
950 Wang, Y., Hu, J., Wang, Y., Ye, W., Zhang, X., Ju, H., Xu, D., Liu, L., Ye, D., Zhang, L., *et al.*
951 (2018). EGFR activation induced Snail-dependent EMT and myc-dependent PD-L1 in
952 human salivary adenoid cystic carcinoma cells. Cell cycle *17*, 1457-1470.
953 Ware, K. E., Garcia-Blanco, M. A., Armstrong, A. J., and Dehm, S. M. (2014). Biologic
954 and clinical significance of androgen receptor variants in castration resistant
955 prostate cancer. Endocr Relat Cancer *21*, T87-t103.
956 Ware, K. E., Somarelli, J. A., Schaeffer, D., Li, J., Zhang, T., Park, S., Patierno, S. R.,
957 Freedman, J., Foo, W. C., Garcia-Blanco, M. A., and Armstrong, A. J. (2016). Snail

promotes resistance to enzalutamide through regulation of androgen receptor activity in prostate cancer. Oncotarget *7*, 50507-50521.
Werden, S. J., Sphyris, N., Sarkar, T. R., Paranjape, A. N., LaBaff, A. M., Taube, J. H., Hollier, B. G., Ramirez-Pena, E. Q., Soundararajan, R., den Hollander, P., *et al.* (2016). Phosphorylation of serine 367 of FOXC2 by p38 regulates ZEB1 and breast cancer metastasis, without impacting primary tumor growth. Oncogene *35*, 5977-5988.
Wu, X., Li, Y., Liu, X., Cao, S., Harrington, S. M., Chen, C., Mansfiled, A. S., Dronca, R. S., Park, S. S., Yan, Y., *et al.* (2018). B7-H1(PD-L1) confers chemoresistance through ERK and p38 MAPK pathway in tumor cells. bioRxiv, 308601.
Yang, L., Pang, Y., and Moses, H. L. (2010). TGF-beta and immune cells: an important regulatory axis in the tumor microenvironment and progression. Trends in immunology *31*, 220-227.
Yoshimura, A., and Muto, G. (2011). TGF-beta function in immune suppression. Current topics in microbiology and immunology *350*, 127-147.
Yu-Lee, L. Y., Yu, G., Lee, Y. C., Lin, S. C., Pan, J., Pan, T., Yu, K. J., Liu, B., Creighton, C. J., Rodriguez-Canales, J., *et al.* (2018). Osteoblast-Secreted Factors Mediate Dormancy of Metastatic Prostate Cancer in the Bone via Activation of the TGFbetaRIII-p38MAPK-pS249/T252RB Pathway. Cancer research *78*, 2911-2924.
Zhang, H., Ye, Y. L., Li, M. X., Ye, S. B., Huang, W. R., Cai, T. T., He, J., Peng, J. Y., Duan, T. H., Cui, J., *et al.* (2017). CXCL2/MIF-CXCR2 signaling promotes the recruitment of myeloid-derived suppressor cells and is correlated with prognosis in bladder cancer. Oncogene *36*, 2095-2104.
Zhang, T. (2018). Expression of immune checkpoints (ICs) on circulating tumor cells (CTCs) in men with metastatic prostate cancer (mPC). Journal of clinical oncology : official journal of the American Society of Clinical Oncology.
Zhang, T., Austin, R. G., Park, S. E., Runyambo, D., Boominathan, R., Rao, C., Bronson, E., Anand, M., Healy, P., George, D. J., *et al.* (2018). Expression of immune checkpoints (ICs) on circulating tumor cells (CTCs) in men with metastatic prostate cancer (mPC). Journal of Clinical Oncology *36*, 5059-5059.
Zhou, B. P., Deng, J., Xia, W., Xu, J., Li, Y. M., Gunduz, M., and Hung, M. C. (2004). Dual regulation of Snail by GSK-3beta-mediated phosphorylation in control of epithelial-mesenchymal transition. Nature cell biology *6*, 931-940.

Figure 1

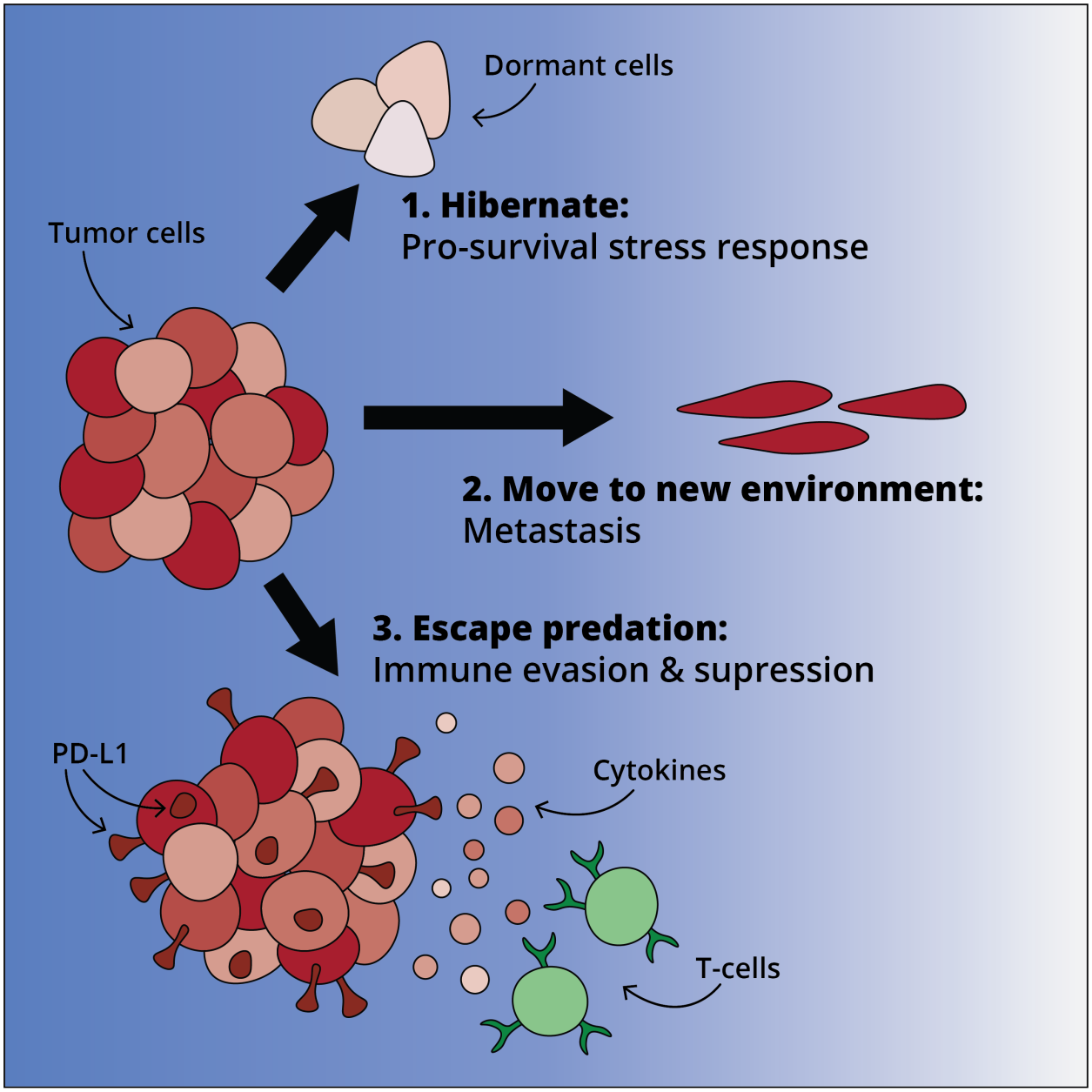
Dormant cells
1. Hibernate:
Pro-survival stress response
Tumor cells
2. Move to new environment:
Metastasis
3. Escape predation:
Immune evasion & supression
PD-L1
Cytokines
T-cells
Unfavorable environment
Favorable environment

Figure 2

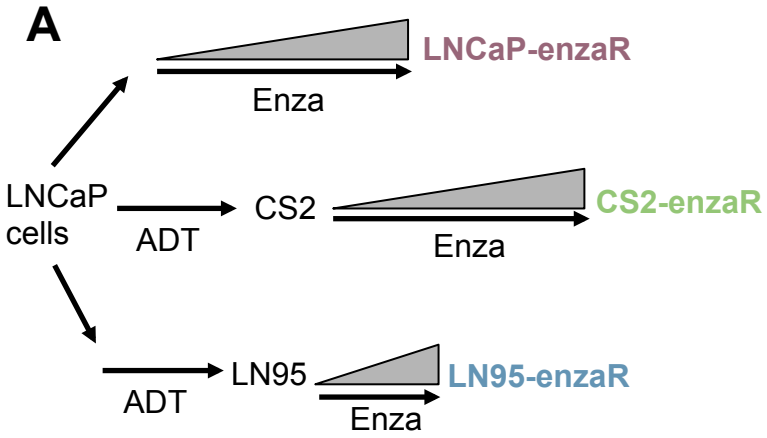

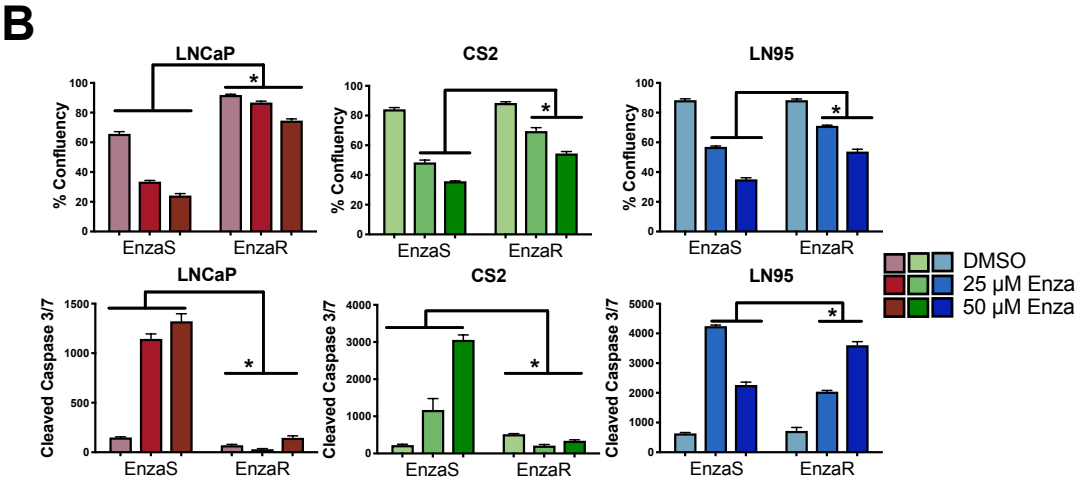

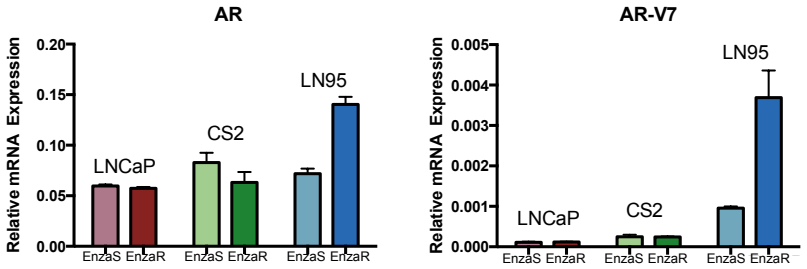

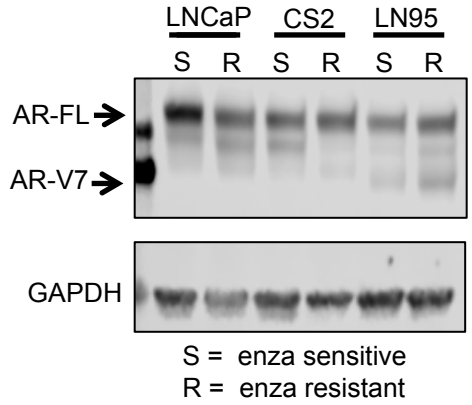

E

		expression				genomic				
Cell Line	Prior ADT	AR	AR-V7	GR	NEPC signature	F876L	AR gain	RB loss	TP53 loss	BRCA2 loss
LNCaP EnzaR	-	+	-	-	-	+	-	-	-	-
CS2 EnzaR	+	+	-	+	-	-	-	+	-	+
LN95 EnzaR	+	+	+	-	-	-	-	-	-	-

Figure 3

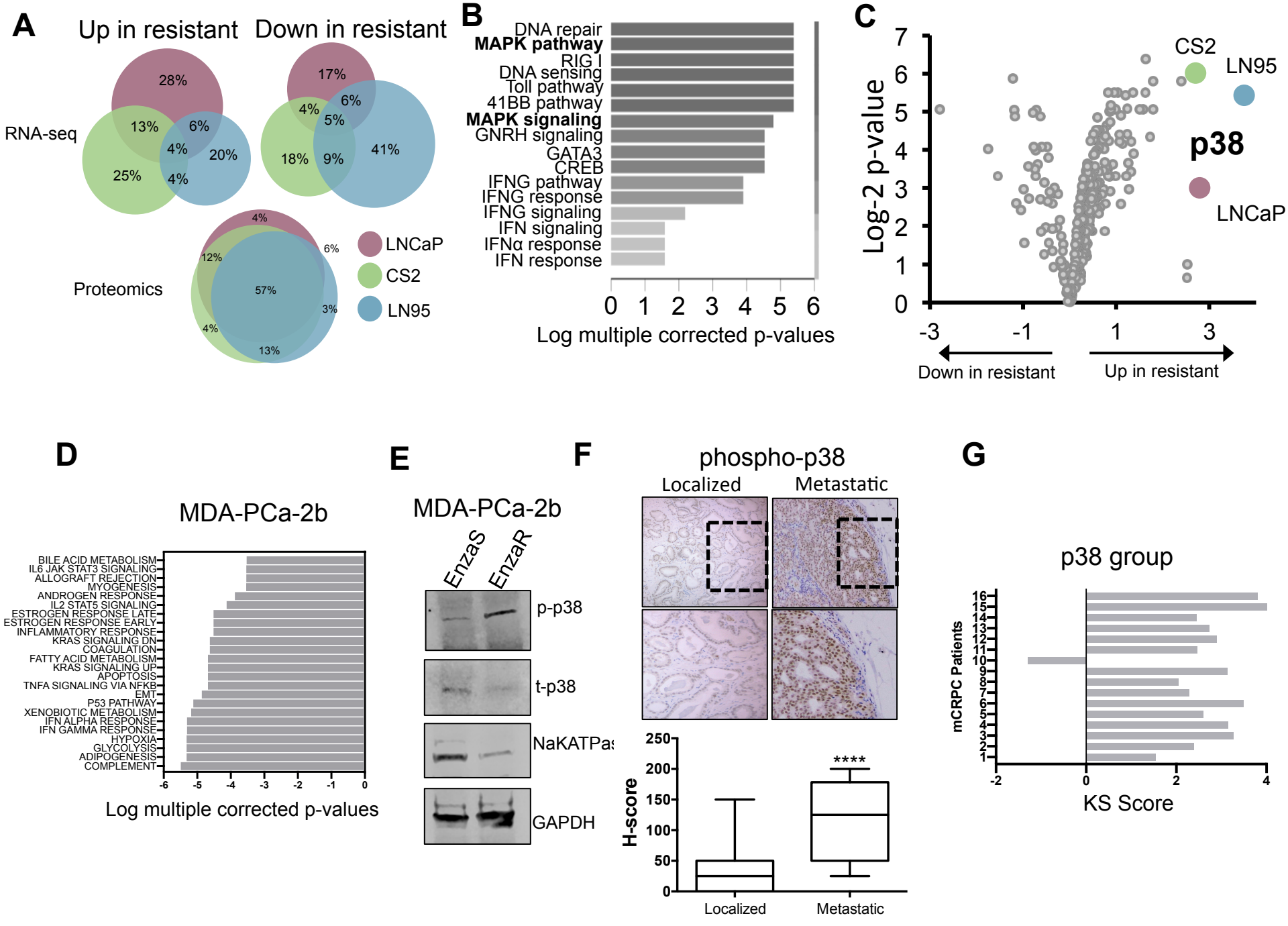
A
Up in resistant
Down in resistant
RNA-seq
28%
13%
6%
4%
20%
25%
4%
17%
6%
4%
5%
18%
9%
41%
Proteomics
4%
6%
12%
57%
3%
4%
13%
LNCaP
CS2
LN95
B
DNA repair
MAPK pathway
RIG I
DNA sensing
Toll pathway
41BB pathway
MAPK signaling
GNRH signaling
GATA3
CREB
IFNG pathway
IFNG response
IFNG signaling
IFN signaling
IFNα response
IFN response
0 1 2 3 4 5 6
Log multiple corrected p-values
C
Log-2 p-value
0 1 2 3 4 5 6 7
CS2
LN95
p38
LNCaP
-3 -1 1 3
Down in resistant
Up in resistant
D
MDA-PCa-2b
BILE ACID METABOLISM
IL6 JAK STAT3 SIGNALING
ALLOGRAFT REJECTION
MYOGENESIS
ANDROGEN RESPONSE
IL2 STAT5 SIGNALING
ESTROGEN RESPONSE LATE
ESTROGEN RESPONSE EARLY
INFLAMMATORY RESPONSE
KRAS SIGNALING DN
COAGULATION
FATTY ACID METABOLISM
KRAS SIGNALING UP
APOPTOSIS
TNFA SIGNALING VIA NFKB
EMT
P53 PATHWAY
XENOBIOTIC METABOLISM
IFN ALPHA RESPONSE
IFN GAMMA RESPONSE
HYPOXIA
GLYCOLYSIS
ADIPOGENESIS
COMPLEMENT
-6 -5 -4 -3 -2 -1 0
Log multiple corrected p-values
E
MDA-PCa-2b
EnzaS
EnzaR
p-p38
t-p38
NaKATPas
GAPDH
F
phospho-p38
Localized
Metastatic
H-score
250
200
150
100
50
0
****
Localized
Metastatic
G
p38 group
mCRPC Patients
16 15 14 13 12 11 10 9 8 7 6 5 4 3 2 1
-2 0 2 4
KS Score

Figure 4

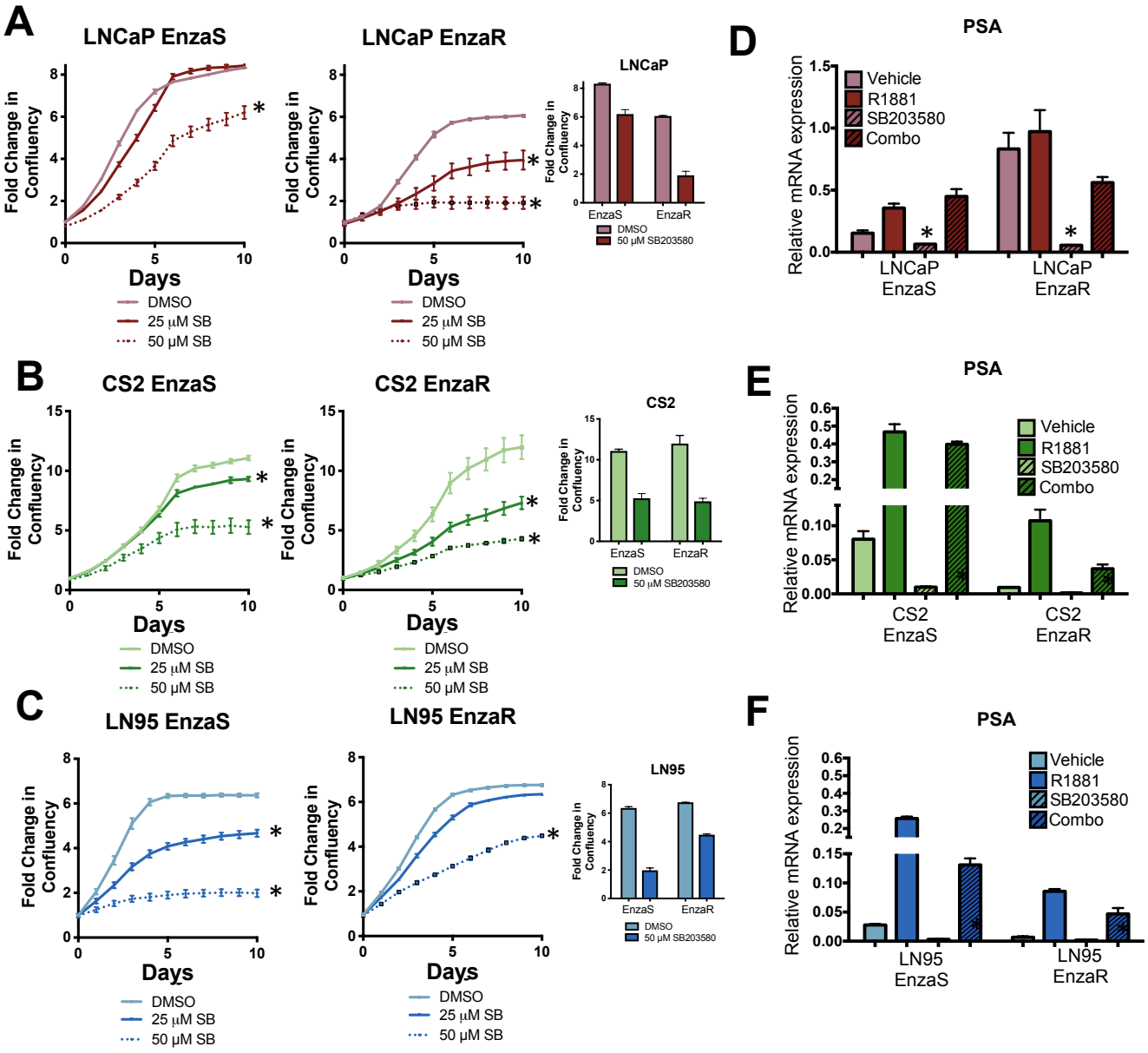
A
LNCaP EnzaS
LNCaP EnzaR
LNCaP
Fold Change in Confluency
Days
DMSO
25 μM SB
50 μM SB
EnzaS
EnzaR
DMSO
50 μM SB203580
B
CS2 EnzaS
CS2 EnzaR
CS2
C
LN95 EnzaS
LN95 EnzaR
LN95
D
PSA
Relative mRNA expression
Vehicle
R1881
SB203580
Combo
LNCaP EnzaS
LNCaP EnzaR
E
CS2 EnzaS
CS2 EnzaR
F
LN95 EnzaS
LN95 EnzaR

Figure 5

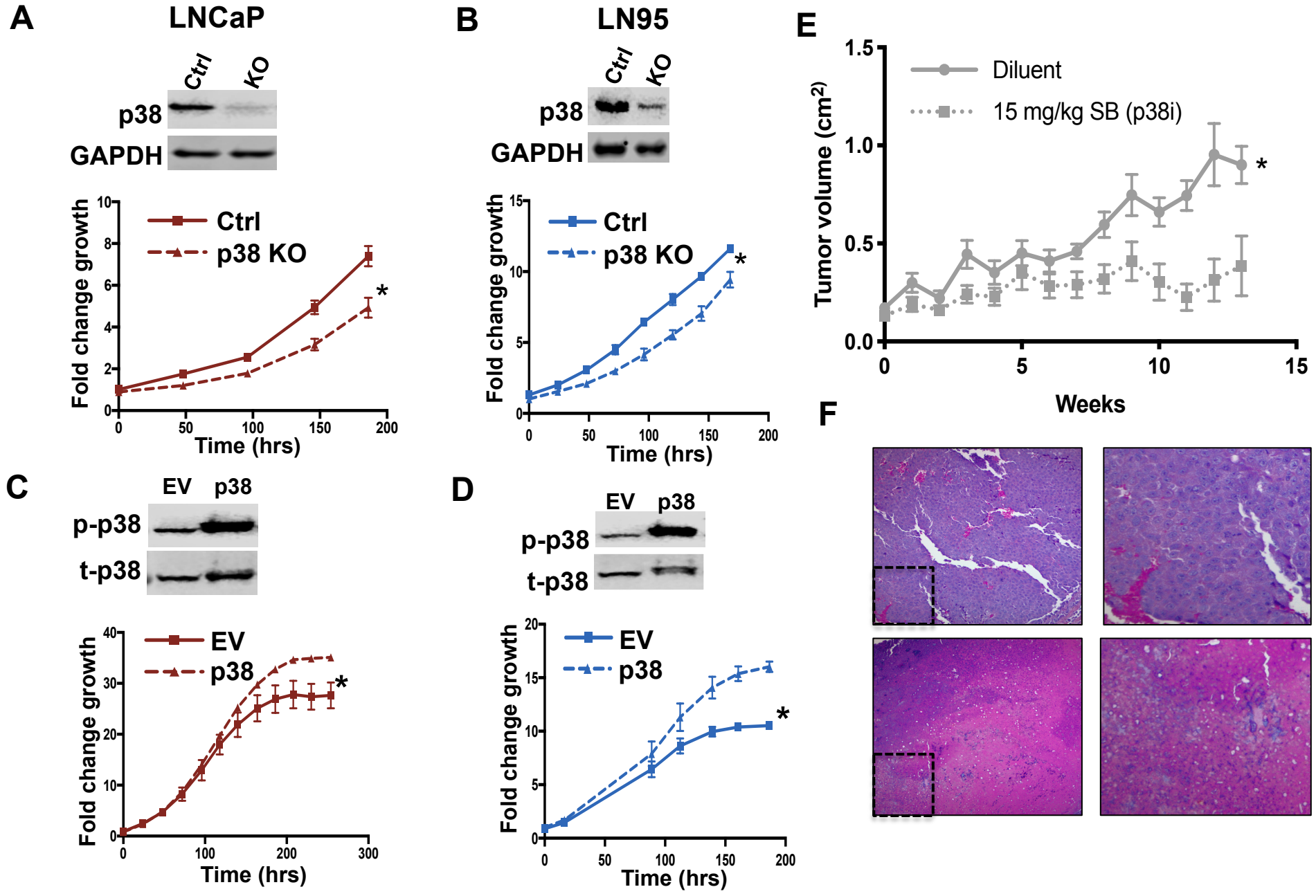
A
LNCaP
Ctrl
KO
p38
GAPDH
Fold change growth
Ctrl
p38 KO
Time (hrs)
B
LN95
C
EV
p38
p-p38
t-p38
D
E
Tumor volume (cm2)
Diluent
15 mg/kg SB (p38i)
Weeks
F

Figure 6

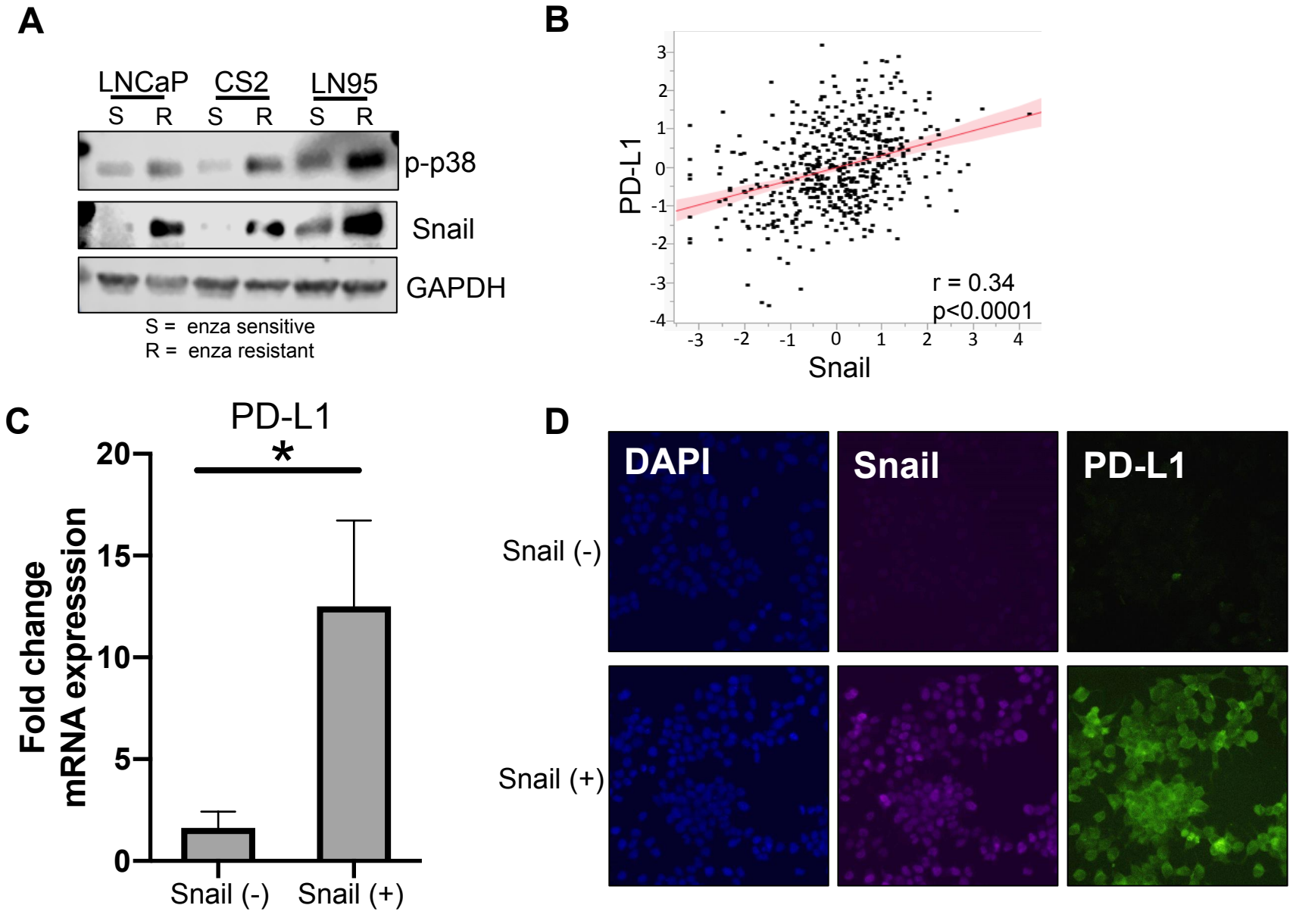
A
LNCaP
CS2
LN95
S
R
S
R
S
R
p-p38
Snail
GAPDH
S = enza sensitive
R = enza resistant
B
PD-L1
Snail
r = 0.34
p<0.0001
C
PD-L1
*
Fold change mRNA expresssion
Snail (-)
Snail (+)
D
DAPI
Snail
PD-L1
Snail (-)
Snail (+)

Figure 7

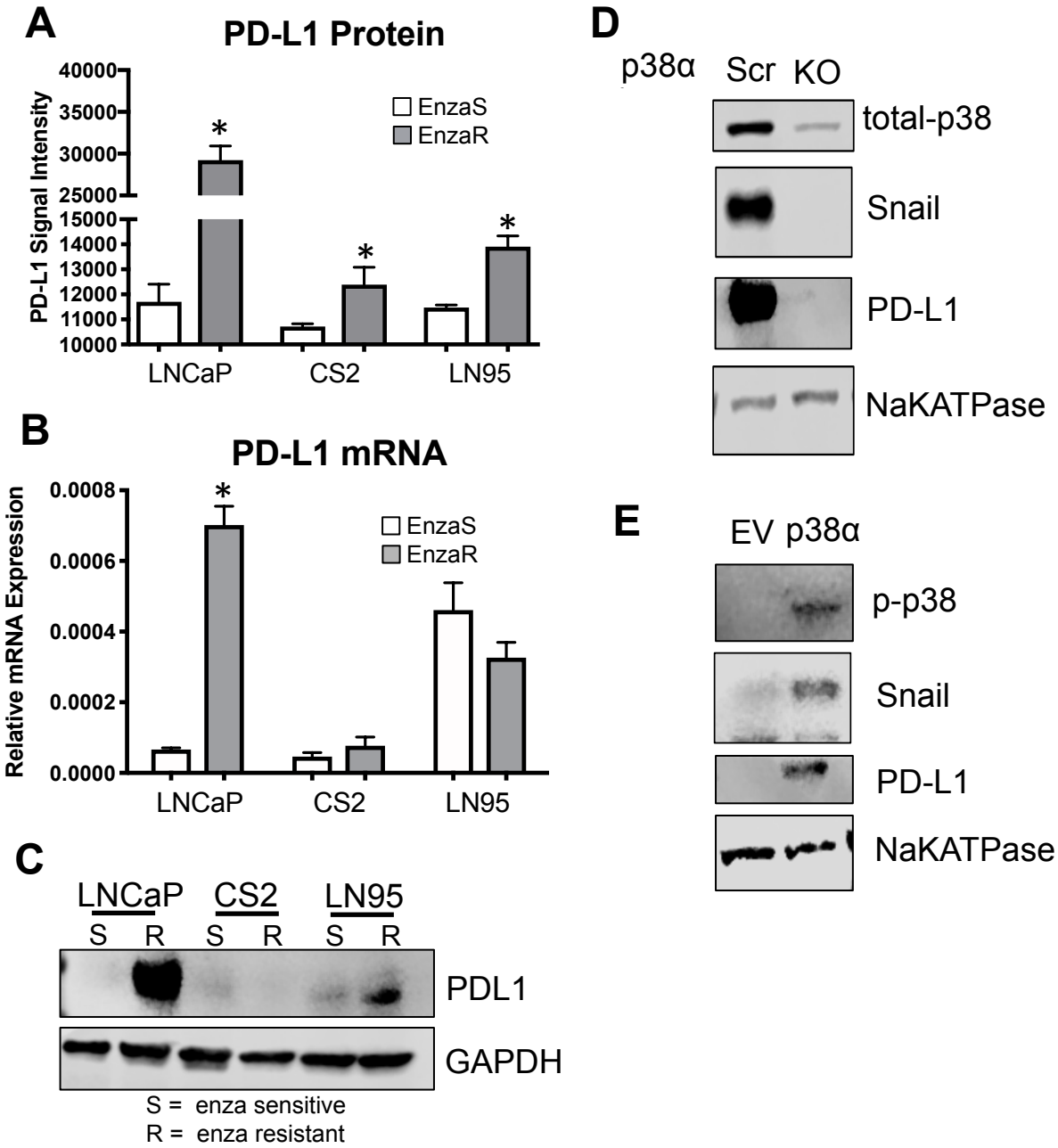
A
PD-L1 Protein
PD-L1 Signal Intensity
40000
35000
30000
25000
15000
14000
13000
12000
11000
10000
EnzaS
EnzaR
LNCaP
CS2
LN95
B
PD-L1 mRNA
Relative mRNA Expression
0.0008
0.0006
0.0004
0.0002
0.0000
C
LNCaP
CS2
LN95
S R S R S R
PDL1
GAPDH
S = enza sensitive
R = enza resistant
D
p38α Scr KO
total-p38
Snail
PD-L1
NaKATPase
E
EV p38α
p-p38
Snail
PD-L1
NaKATPase
F
Enzalutamide-induced loss of AR signaling
p38 inhibition
1. Alter resource acquisition:
Pro-survival stress response
p38
AR inhibition
Enzalutamide
Snail
PD-L1
2. Move to new environment:
Metastasis
PD-1/PD-L1
blockade
3. Escape predation:
Immune evasion & supression
Unfavorable
environment
Favorable
environment